Journal of Thermal Analysis and Calorimetry (2023) 148:3311–3323
https://doi.org/10.1007/s10973-023-11985-w

Non-isothermal crystallization kinetics of polypropylene homopolymer/impact copolymer composites

Pixiang Wang[1] · Yifen Wang[2] · Xueqi Wang[3] · Yucheng Peng[3] · Shaoyang Liu[1]

Received: 12 May 2022 / Accepted: 22 January 2023 / Published online: 24 February 2023

Abstract

Crystallization kinetics of an isotactic homopolymer polypropylene (HPP), an impact copolymer polypropylene (ICPP), and their composites were studied in this work. The Avrami–Jeziorny and Mo models successfully described the crystallization process. When the ICPP content increased, the crystallization rate first increased and then decreased with the highest crystallization rate at the ICPP content of 60 mass%. The nucleation activity kept increasing with the rise of the ICPP content, demonstrating that the rubber phase in the ICPP acted as a nucleating agent and prompted the nucleation process. The decrease in crystallization rate when the ICPP content was higher than 60 mass% might be caused by the decrease in chain mobility and the increase in crystal–crystal interactions. When the ICPP content exceeded 60 mass%, the crystallization activation energy increased evidently, indicating lower polymer chain mobility. Meanwhile, the Avrami exponent, n, decreased, suggesting limited crystal growth space and higher crystal–crystal interactions. The nucleation activity showed high correlations to the mechanical and thermal properties of the materials. The Avrami exponent also had relatively high correlations to these properties. The results improved the understanding of the crystallization behaviors of the HPP–ICPP composites and helped predict their potential mechanical behavior changes.

Keywords Polypropylene · Crystallization kinetics · Avrami–Jeziorny model · Mo model · Crystallization activation energy · Nucleation activity

Introduction

Polypropylene (PP) has been widely used as a thermoplastic resin in various fields including packaging, appliances, construction and automobile due to its outstanding physical and mechanical properties [1]. PP has occupied almost 20% of the market shares and continues to grow [2, 3]. Isotactic homopolymer polypropylene (HPP) in a semicrystalline solid form, which contains only propylene monomer and the methyl groups are arranged on the same side of the main chain, is the most widely utilized general-purpose PP and is offered by many suppliers in the market [3]. However, the relatively low impact strength and high brittleness of HPP limit its applications. Blending or copolymerizing HPP with elastomers/rubbers can generate various types of impact copolymer PP (ICPP) with improved impact resistance. This is an effective and practical modification, which has been successfully commercialized on large scales [4–6]. The characteristics of the elastomer/rubber phase including shape, size, distribution, and loading level, have significant influences on ICPP's impact strength and other properties [3, 7].

Different applications desire different impact strengths. Therefore, various ICPP products have been manufactured to satisfy different needs. But the complicated material portfolio could increase supply chain difficulties, and the complex chemical compositions could hamper recycling and reusing of the materials. Our previous study successfully demonstrated a strategy of mixing an HPP and an ICPP with high

✉ Yucheng Peng
yzp0027@auburn.edu

✉ Shaoyang Liu
lius@troy.edu

[1] Center for Materials and Manufacturing Sciences, Departments of Chemistry and Physics, Troy University, 315 Math and Science Complex, Troy, AL 36082, USA

[2] Biosystems Engineering Department, Auburn University, Auburn, AL 36849, USA

[3] College of Forestry, Wildlife, and Environment, Auburn University, Auburn University, 520 Devall Drive, Auburn, AL 36849, USA

impact strength to obtain composites with impact strengths in between [8]. The mixtures show graduate changes in impact strength, tensile properties, and flexural properties depending on the HPP–ICPP composition. The strategy could shorten the portfolio to two basic materials, reduce inventory, and simplify the chemical profile for recycling.

Degree of crystallinity, nucleation mechanism, and crystalline structure strongly affect the properties of HPP, ICPP, and their mixtures [9, 10]. In general, the surface of the filler particles (elastomers/rubbers) in ICPP may act as nucleation agents and affect the amount and/or type of the crystal phase in the composites notably, which could significantly influence the mechanical properties, such as tensile and impact strength [11]. Thus, it is essential to study both the nucleation and crystal growth processes to understand the crystal phase and help optimize the properties of HPP, ICPP, and their composites.

Kinetic parameters of non-isothermal crystallization can provide rich information about the process [12, 13]. Several empirical and theoretical models, such as Avrami, Ozawa, and Mo equations, have been developed to describe different non-isothermal crystallization processes [14–17]. The Avrami equation has a parameter indicating crystallization rate, and the Avrami exponent, n, is related to nucleation mechanism and crystal growth geometry. The Ozawa model adds the cooling rate into account. The Mo equation combines the Avrami and Ozawa equations and deduces a parameter with definite physical meaning, describing the necessary cooling rate to reach a given degree of crystallinity in a unit time. These three models have been widely used to elucidate crystallization processes of polymers and their composites [18–24].

The main scope of this work is to explore the effects of ICPP content on the crystallization behaviors of HPP-ICPP composites made by direct thermal mixing with commercial grade materials. The crystallization kinetics study helps understand whether the thermal mixing process impacts the polymer crystalline structure and kinetics in the plastic converting process, which provides critical information for formulation design during the product development. The research outcomes are also crucial to predicting the potential mechanical behavior change of the mixtures when different ratios of HPP to ICPP are used. Composites with 20, 40, 60, and 80 mass% of the ICPP were prepared. Crystallization processes at cooling rates from 5 to 15 °C min^{-1} were investigated. Crystallization kinetics of the ICPP, HPP and their composites were analyzed using the Avrami equation modified by the Jeziorny method, Ozawa equation, and Mo equation. Furthermore, the apparent crystallization activation energy and nucleation activity were calculated based on the differential scanning calorimetry (DSC) analyses using the Kissinger and Dobreva Gutzow methods, respectively.

Experimental

Materials

Polymer pellets of an HPP (ExxonMobil™ PP1264E1) and an ICPP (ExxonMobil™ PP7684KNE1) were donated by ExxonMobil Chemical Company (Houston, TX). Both the HPP and ICPP had a density of 0.9 g cm^{-3}. The melt mass-flow rates (MFR) of the HPP and ICPP were 20 and 19 g per 10 min, respectively.

Sample preparation

Thermal mixing of the HPP and ICPP was performed using a C.W. Brabender mixer (CWB-2128, Hackensack, NJ) at 200 °C. The two roller blades of the mixer, simulating the twin-screw extruder mixing action, counter-rotated at 60 rpm. The loading levels of the ICPP used in this study were 20, 40, 60, and 80 mass% based on the total mass of the composites. The HPP and ICPP pellets were first dry blended and then melted in the mixer at 200 °C. Next, the solidified mixtures were ground into pellets using a low-speed granulator (Shini Plastic Technologies Inc., Willoughby, OH) with a sieve size of 3 mm. The samples of pure HPP and ICPP were also prepared using the same procedure before the DSC analysis.

DSC analysis

Differential scanning calorimetry (DSC) analysis was carried out with a DSC-250 calorimeter (TA Instruments, DE, USA). About 10 to 15 mg of each sample was sealed into Tzero pans. The sample was first heated from 40 to 200 °C at a rate of 10 °C min^{-1} and maintained at 200 °C for 2 min to remove thermal history. Then, the non-isothermal crystallization was performed at a series of cooling rates (5, 7.5, 10, 12.5, and 15 °C min^{-1}) to obtain the curves from 200 to 40 °C, respectively. The samples were again heated to 200 °C at 10 °C min^{-1} to analyze their melting behaviors. The melting enthalpy was obtained from the melting peak area of the second heating cycle. The crystallinity was calculated using the latent heat of fusion of 100% crystalline polymer (207 J g^{-1} for polypropylene) divided by the melting enthalpy [25, 26]. All tests were performed under an N_2 atmosphere (50 mL min^{-1}). Each sample was measured in triplicates. All data analyses were performed with TRIOS software (TA Instruments, DE, USA).

Results and discussion

Crystallization behavior

Figure 1 depicts the DSC cooling curves of the non-isothermal crystallization for the HPP, ICPP, and the composites. The crystallization onsets and peaks shifted to higher temperatures as the cooling rate decreased. Lower cooling rates, which could provide more nucleation time and more energy for polymer chains to move around, were considered better crystallization conditions for nucleation and crystal growth [27, 28].

At the same cooling rate, the onset and peak temperatures of crystallization increased with the increase of the ICPP content (Fig. 2a, b). The results indicated that the rubber phase in the ICPP might act as a heterogeneous nucleating agent and facilitate the crystallization process, especially during the early nucleation stage. However, the elevated nucleation rate could lead to stronger crystal-crystal interaction and less perfect crystallization when compared to the neat HPP. Therefore, the crystallinity

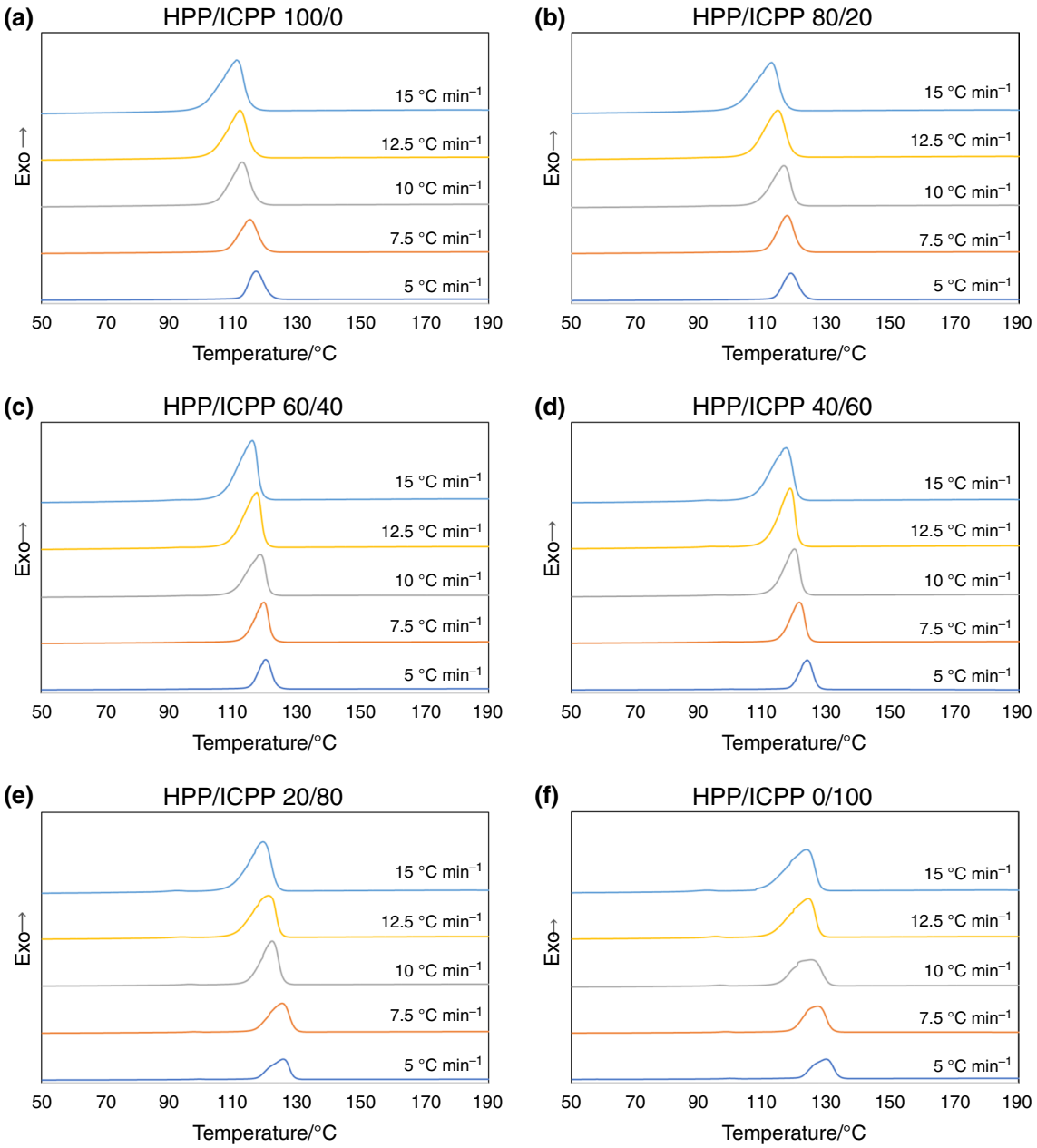

Fig. 1 DSC cooling curves at different cooling rate

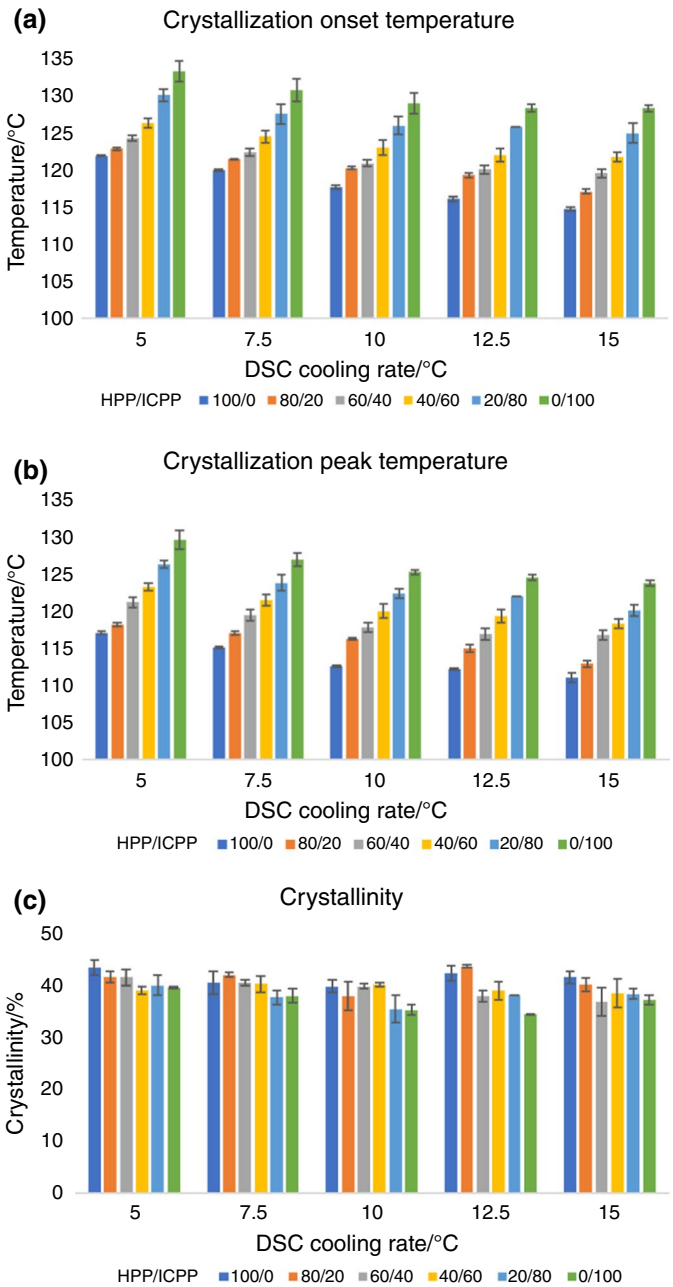

Fig. 2 Non-isothermal crystallization behavior of HPP, ICPP and the composites. **a**: crystallization onset temperature, **b**: crystallization peak temperature, and **c**: crystallinity

tended to decrease with the increase of the ICPP content at the same cooling rate, as shown in Fig. 2c. This phenomenon was more pronounced at higher cooling rates. A similar phenomenon was observed in a previous report [29].

The relative degree of crystallinity (X_t) as a function of temperature (T) can be described with the following Eq. 1. In a non-isothermal crystallization process, crystallization time (t) can be calculated by Eq. 2.

$$X_t = \frac{\int_{T_0}^{T} \left(\frac{dH_c}{dT}\right) dT}{\int_{T_0}^{T_\infty} \left(\frac{dH_c}{dT}\right) dT} \tag{1}$$

$$t = \frac{|T_0 - T|}{\Phi} \tag{2}$$

where T_0 and T_∞ are the initial and final temperatures of crystallization, respectively. dH_c is the enthalpy of crystallization released during an infinitesimal temperature interval. T represents the temperature at the crystallization time t, and Φ is the cooling rate.

The evolutions of the relative degree of crystallinity (X_t) during the non-isothermal crystallization processes are presented in Fig. 3. All curves were sigmoid, indicating that the crystallization accelerated when nuclei gradually formed at the beginning of the process and slowed down when the process was close to the finish. All samples displayed a similar tendency: the curves shifted to the right on the time axis as the cooling rate decreased, especially when the cooling rate dropped from 10 to 5 °C min^{-1}. A longer leading time under a lower cooling rate was because the nucleation became slower.

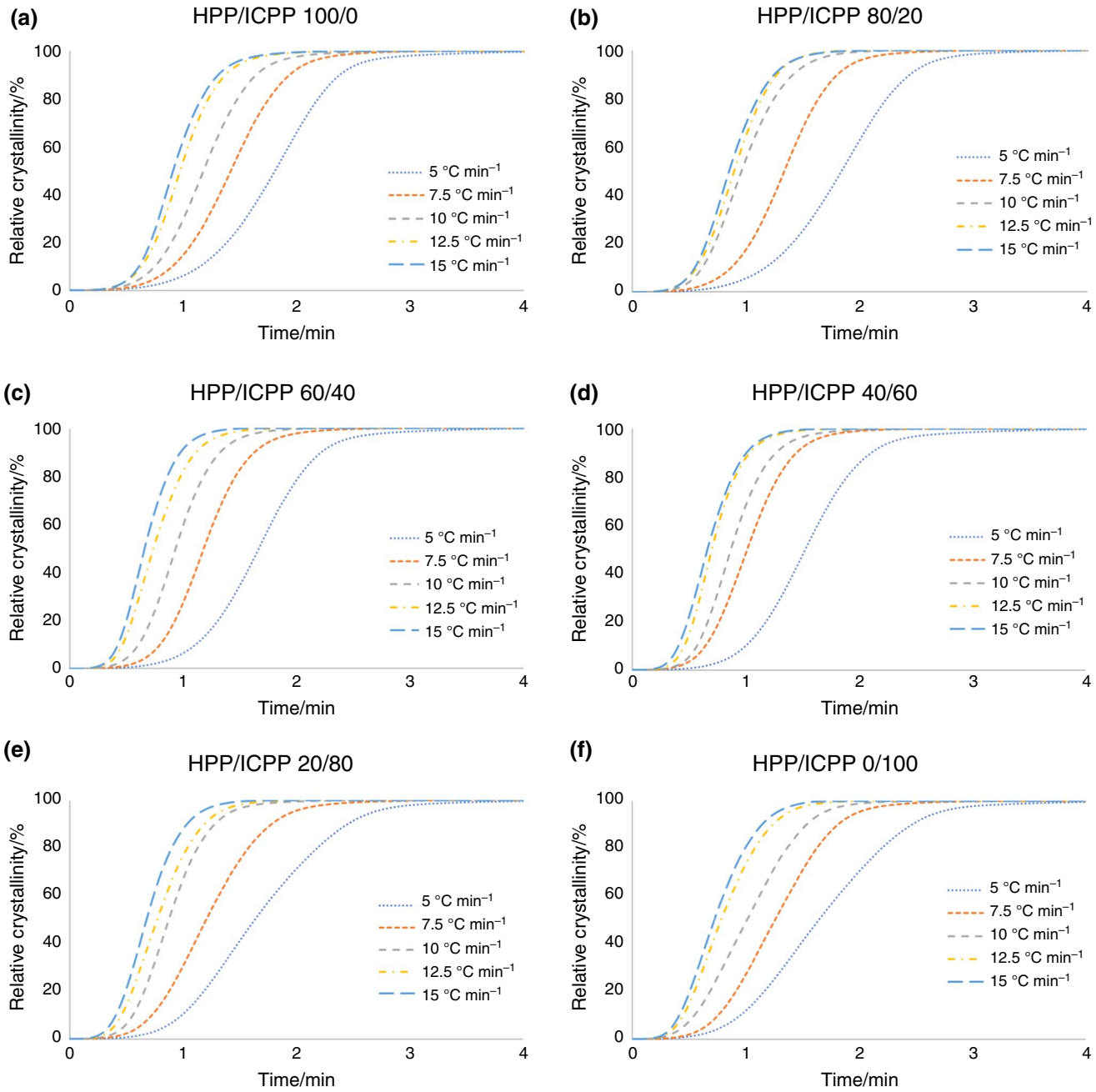

Fig. 3 The relationships of relative crystallinity and time at different cooling rate

Non-isothermal crystallization kinetics

Kinetic analyses were carried out with three widely accepted models, including the modified *Avrami* (*Jeziorny theory*), *Ozawa*, and *Mo* equations [21–24], to provide more insights of the non-isothermal crystallization behavior of the samples.

Jeziorny theory

The widely used Avrami equation for isothermal crystallization was described in Eq. 3. With the assumption of constant crystallization temperature, taking the natural logarithm of both sides of Eq. 3 can generate Eq. 4 for linear regression.

$$1 - X_t = \exp(-Z_t t^n) \tag{3}$$

$$\ln\left[-\ln\left(1 - X_t\right)\right] = \ln Z_t + n\ln t \tag{4}$$

where Z_t is the crystallization rate constant, and n is the Avrami exponent, which depends on the nucleation mechanism and crystal growth dimension.

The crystallization half-time ($t_{1/2}$), which is the duration required to achieve 50% crystallization, can be calculated with Eq. 5 [30]. A smaller $t_{1/2}$ suggests a quicker crystallization.

$$t_{1/2} = \left(\frac{\ln 2}{Z_t}\right)^{1/n} \tag{5}$$

Considering the effect of cooling rate, Jeziorny defined a new crystallization parameter Z_c to describe practical non-isothermal crystallization at different cooling rates (Φ), as shown in Eq. 6. The Z_c value indicates the crystallization rate [22, 31].

$$\ln Z_c = \frac{\ln Z_t}{\Phi} \tag{6}$$

Figure 4 illustrates the plots of ln[-ln(1-X_t)] against ln t, and the kinetic parameters derived from the fitting lines based on the Jeziorny theory are summarized in Table 1. Under all cooling rates, the fitting lines overlapped on the experimental data points well, and all R^2 were higher than 0.96, suggesting the Jeziorny model described the crystallization process in this case. For the same sample, the Z_c value increased with the increase in the cooling rate because the crystallization process was quicker when cooling faster. When comparing different samples, the Z_c value increased with the increase in the ICPP content up to 60% at most cooling rates, suggesting quicker crystallization. However, as the ICPP content exceeded 60%, the Z_c value began to decrease, implying the accelerating effect started to fade. The highest crystallization rate at 60% ICPP agreed with the result of crystallization half-time ($t_{1/2}$) (Table 1) and the observation in Fig. 2. The neat ICPP had a larger Z_c than the neat HPP, indicating the ICPP crystallized quicker than the HPP.

The value of n depends on the crystallization mechanism and crystal growth dimension [32, 33]. For values of $2 < n < 3$, the growth occurs in two dimensions with lamella geometry; for $3 < n < 4$, the growth takes place in three dimensions with sphere geometry. The n values for the neat HPP were above 3 (Table 1), suggesting the crystal growth tended to occur in three dimensions. When the ICPP was added to the HPP, the n values increased at the beginning, implying the crystals more likely grew into a spherulitic structure. For the cooling rates of 5.0, 12.5, and 15.0 °C min^{-1}, the highest n values were found when 20% of the ICPP was added. For the cooling rates of 7.5 and 10.0 °C min^{-1}, the highest n values were observed when 40% of the ICPP presented. When the ICPP content continued to increase, the n values gradually decreased. The n value of the neat ICPP at the cooling rate of 5.0 °C min^{-1} even dropped below 3, indicating the crystals could grow in two dimensions and some lamella structures could be formed. The decrease in n value might be caused by the limited crystal growth space and the increasing crystal-crystal interactions when large amounts of ICPP were added and evidently promoted nucleation. The nucleation effect of the ICPP will be discussed in detail in a later section. The evolution of the n value was similar to a biochar/polypropylene composite, whose n value first increased and then decreased with the increase of the content of biochar prepared by pyrolysis at 400 °C [20]. It was reported that when the value of n was greater than 4, the crystals could form complex spherulites [34]. In this study, however, all the n values were well below 4, indicating that simple spherulites were mainly formed in the crystallization processes. Moreover, the value of n was also affected by the cooling rate of the same samples. Higher n values were observed with larger cooling rates, which might be related to the increase in athermal nucleation [15].

Ozawa equation

Since cooling rate (Φ) is an important factor in crystallization process, Ozawa incorporated it by modifying the Avrami equation as expressed in Eq. 7. To calculate the rate constant $K(T)$, Eq. 7 could be converted to Eq. 8 in the double-natural logarithmic form.

$$1 - X_t = \exp\left[\frac{-K(T)}{\Phi^m}\right] \tag{7}$$

$$\ln\left[-\ln\left(1 - X_t\right)\right] = \ln K(T) - m\ln\Phi \tag{8}$$

where $K(T)$ was the crystallization rate constant and m is the Ozawa exponent. Table 2 shows the kinetic parameters

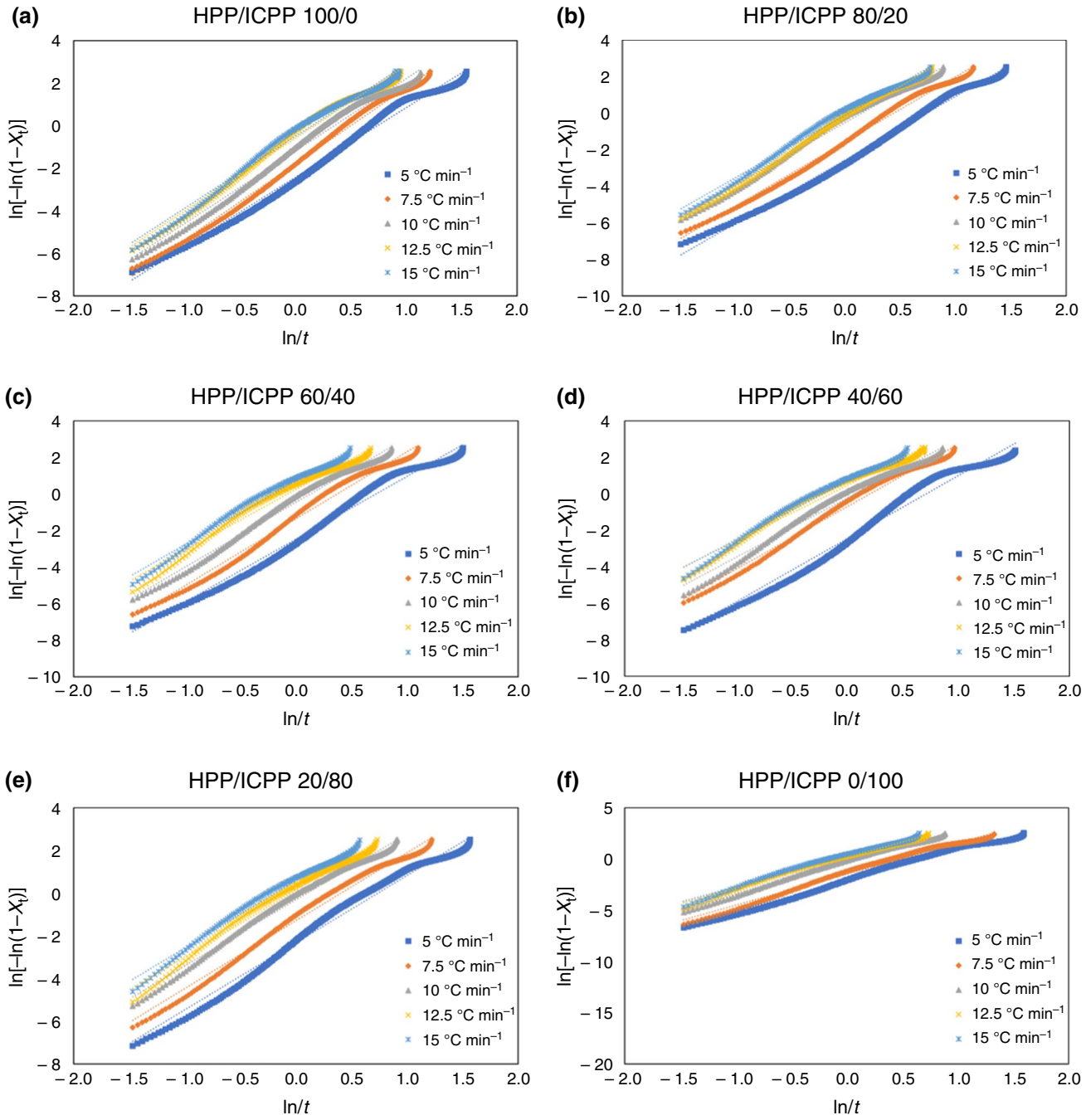

Fig. 4 Plots of ln(-ln(1−X_t)) versus ln t from the Jeziorny theory for non-isothermal crystallization

obtained from Eq. 8 by linear regression. Compared to those from the Jeziorny theory, the fitting lines based on the Ozawa equation showed evident deviations from linearity with notably lower R^2 for the composites. The results suggest that the Ozawa equation might not be suitable to describe the non-isothermal crystallization of the composites studied in this work.

Table 1 Non-isothermal crystallization kinetic parameters determined from Jeziorny theory

HPP/ICPP ratio	Φ/°C min^{-1}	Zt/min^{-n}	Zc/min^{-n} K^{-1}	Avrami exponent n	R^2	$t_{1/2}$
100/0	5.0	0.075	0.015	3.29	0.99	1.96
	7.5	0.188	0.025	3.56	0.99	1.44
	10.0	0.297	0.030	3.36	0.99	1.29
	12.5	0.533	0.043	3.48	0.98	1.08
	15.0	0.635	0.042	3.35	0.98	1.03
80/20	5.0	0.077	0.015	3.49	0.99	1.88
	7.5	0.221	0.029	3.61	0.99	1.37
	10.0	0.589	0.059	3.47	0.99	1.05
	12.5	0.703	0.056	3.55	0.99	1.00
	15.0	0.988	0.066	3.47	0.99	0.90
60/40	5.0	0.105	0.021	3.39	0.98	1.74
	7.5	0.262	0.035	3.76	0.99	1.30
	10.0	0.686	0.069	3.49	0.98	1.00
	12.5	1.017	0.081	3.28	0.96	0.89
	15.0	2.136	0.142	3.38	0.98	0.72
40/60	5.0	0.112	0.022	3.26	0.97	1.75
	7.5	0.471	0.063	3.43	0.98	1.12
	10.0	0.756	0.076	3.30	0.98	0.97
	12.5	1.535	0.123	3.22	0.97	0.78
	15.0	1.932	0.129	3.20	0.98	0.73
20/80	5.0	0.106	0.021	3.15	0.98	1.81
	7.5	0.273	0.036	3.31	0.98	1.33
	10.0	0.709	0.071	3.25	0.98	0.99
	12.5	1.121	0.090	3.13	0.98	0.86
	15.0	1.779	0.119	3.15	0.99	0.74
0/100	5.0	0.099	0.020	2.98	0.98	1.92
	7.5	0.224	0.030	3.07	0.99	1.44
	10.0	0.702	0.070	3.16	0.99	1.00
	12.5	0.934	0.075	3.05	0.99	0.91
	15.0	1.364	0.091	3.02	0.99	0.80

Table 2 Non-isothermal crystallization kinetic parameters determined from Ozawa equation

HPP/ICPP ratio	ln$K(T)$	m	R^2
100/0	6.76	− 5.31	0.99
80/20	7.11	− 4.81	0.93
60/40	7.25	− 4.29	0.90
40/60	7.16	− 3.68	0.95
20/80	3.83	− 1.68	0.89
0/100	3.71	− 1.37	0.98

Mo equation

In order to describe the non-isothermal crystallization process more precisely, Mo and co-workers proposed a combination of the Avrami and Ozawa equations (Eq. 9) [14].

$$\ln\Phi = \ln F(T) - \alpha \ln t \tag{9}$$

where $F(T) = [K(T)/Z_t]^{1/m}$, which represents the cooling rate required to achieve a defined degree of crystallinity at unit crystallization time, and $\alpha = n/m$, which is the ratio of Avrami exponent n to the Ozawa exponent m.

Figure 5 presents the plots of ln Φ versus ln t, and the fitting results are listed in Table 3. The plots showed good linearity, and the R^2 was greater than 0.97 for most of the samples, demonstrating that the Mo equation successfully described the crystallization processes of both the neat polymers and the composites. The α and $F(T)$ values were determined from the slopes and intercepts of the fitted lines, respectively. The values of α varied in a small range from 1.10 to 1.58, similar to those reported in a previous study [21]. The $F(T)$ value is related to the crystallization rate. A higher $F(T)$ value implies a slower crystallization process. The $F(T)$ values increased with the increase of relative

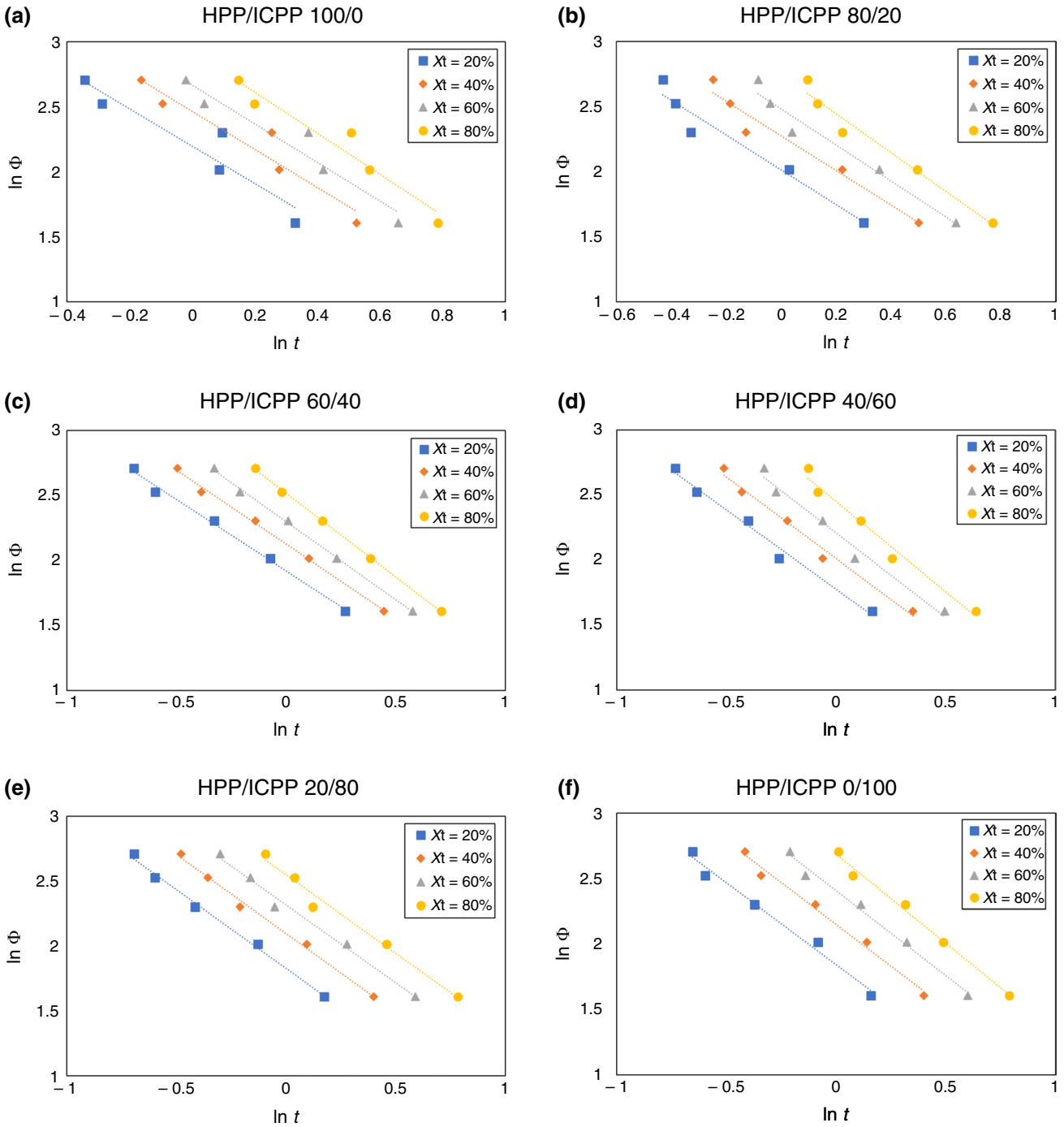

Fig. 5 Plots of ln Φ versus ln t from the Mo's method for non-isothermal crystallization

crystallinity (X_t) for all the samples because the crystallization became more and more difficult as the crystallization progressed. When comparing at the same X_t, the $F(T)$ value kept decreasing until up to 60% of ICPP was added, suggesting the ICPP facilitated the crystallization process. However, when the ICPP content exceeded 60%, the $F(T)$ value began to increase, indicating the acceleration effect diminished, as predicted by the Jeziorny theory. The results of the crystallization rate are in agree with those from the Jeziorny theory. Such a phenomenon might be related to the nucleation effect of the rubber phase in the ICPP and the subsequent crystal growth. The added ICPP provided extra nucleation sites and promoted the nucleation process. But the large number of crystal nuclei created by the ICPP could cause stronger crystal-crystal interaction and affect the polymer chains' mobility, which hindered the crystal growth

Table 3 Non-isothermal crystallization kinetic parameters determined from Mo equation

HPP/ICPP ratio	X_t/%	$F(T)$	α	R^2
100/0	20	9.00	1.44	0.99
	40	11.77	1.46	0.99
	60	14.42	1.49	0.99
	80	18.74	1.58	0.99
80/20	20	7.50	1.34	0.95
	40	9.73	1.35	0.96
	60	11.99	1.38	0.96
	80	15.56	1.49	0.97
60/40	20	6.82	1.10	0.99
	40	8.37	1.14	1.00
	60	9.96	1.20	1.00
	80	12.36	1.29	1.00
40/60	20	5.92	1.22	0.99
	40	7.48	1.26	0.99
	60	9.12	1.30	0.98
	80	11.62	1.39	0.98
20/80	20	6.22	1.22	0.99
	40	8.15	1.21	0.99
	60	10.14	1.20	0.99
	80	12.79	1.19	0.98
0/100	20	6.33	1.25	0.98
	40	8.60	1.28	0.99
	60	11.12	1.29	0.99
	80	14.73	1.36	0.99

in the later stage [30]. Therefore, a maximum crystallization rate at 60% ICPP was observed. More details regarding polymer chain movement and nucleation activity will be discussed in the following two sections.

Activation energy of crystallization

Crystallization activation energy (ΔE) is the energy required for the phase transformation to occur. It is related to polymer chain mobility and needs to be investigated to better understand the crystallization process. Different mathematical methods have been proposed to calculate the ΔE, including Kissinger, Vyazovkin, and Friedman models [22]. In this work, the popular Kissinger model was employed [35], which can be described in Eq. 10.

$$d\left[\ln\left(\frac{\Phi}{T_p^2}\right)\right] = -\frac{\Delta E}{R}d\left(\frac{1}{T_p}\right) \tag{10}$$

where R is the ideal gas constant (8.314 J K^{-1} mol^{-1}) and T_p is the peak crystallization temperature (in K). By plotting ln (Φ/T_p^2) versus $1/T_p$, the data can be fitted by a straight line, from which ΔE can be calculated by multiplying the slope by the negative value of R. Table 4 presents the ΔEs and regression coefficients (R^2). Most R^2 of the samples were greater than 0.97, which demonstrated a good linear relationship and suggested that the Kissinger equation could accurately describe the crystallization process in this work. Negative activation energies were obtained because the crystallization rate increased when the temperature decreased [21, 22].

The ΔE of the neat HPP was − 225.12 kJ mol^{-1}, which is consistent with a previous report (− 221.78 kJ mol^{-1} [21]). The ICPP had a comparable ΔE (− 229.97 kJ mol^{-1}), which might suggest that the polymer molecules in the ICPP and HPP had similar chain mobilities. When the ICPP was added to the HPP, the ΔE decreased evidently, implying easier chain motion. The lowest ΔEs were observed when the ratios of the two types of polymers were close to 1. A better chain mobility could facilitate crystal growth. The evolution of ΔE roughly agreed with the changes of crystallization rate of the composites. The effects of ΔE on the crystallization rate will be further discussed in combination with nucleation activity in the next section.

Crystal nucleation activity

Dobreva and Gutzow proposed a simple method to evaluate nucleation activity [36]. According to this method, the relationships between Φ (cooling rate) and ΔTp (the difference between the melting and crystallization peak temperatures corresponding to the DSC curve) can be presented with Eqs. 11 and 12 for homogeneous and heterogeneous samples, respectively.

Table 4 Non-isothermal crystallization activation energy and nucleation activity values

HPP/ICPP ratio	Activation energy		Nucleation activity			
	ΔE/kJ mol^{-1}	R^2	B^*	B	Ψ	R^2
100/0	− 225.12	0.98		10847.34		0.93
80/20	− 261.64	0.91	9860.95		0.91	0.90
60/40	− 298.68	0.98	9829.22		0.91	0.90
40/60	− 295.69	1.00	8150.72		0.75	0.97
20/80	− 246.88	0.97	7810.56		0.72	0.98
0/100	− 229.97	0.99	5564.33		0.51	0.95

$$\ln\Phi = A - \frac{B}{2.3\Delta T_p^2} \tag{11}$$

$$\ln\Phi = A - \frac{B^*}{2.3\Delta T_p^2} \tag{12}$$

where A, B, and B^* are constants. By plotting ln Φ versus $-1/(2.3\Delta T_p^2)$, the data could be fitted by a straight line, from which A and B (or B^*) could be calculated from the intercept and slope, respectively. The nucleation activity (Ψ) could be calculated by the ratio of B^* and B:

$$\Psi = B*/B \tag{13}$$

The B, B^*, and Ψ are also shown in Table 4. According to the theory, if the nucleation activity of the added dispersed phase (foreign matter) is sufficiently high, the Ψ value should be close to 0. Conversely, if the added dispersed phase has no nucleation activity, the Ψ will be 1 [21, 36]. In this work, all Ψ values were lower than 1, suggesting the rubber phase in the ICPP acted as a nucleating agent. The Ψ value tended to decrease with the increase in the ICPP content implying that the nucleation effect was strengthened by the presence of more ICPP.

Crystallization of polymers, mainly consisting of nucleus formation and crystal growth, is a process associated with the partial alignment of their molecular chains. The polymer's apparent crystallization rate is affected by both nucleation and crystal growth rate. The addition of a heterogeneous nucleating agent can significantly increase the nucleation rate. At the same time, the presence of a nucleating agent may negatively affect crystal growth by hampering the movement of matrix polymer chains and increasing crystal–crystal interactions [21, 30]. The crystal growth prefers a higher polymer chain mobility, which is corresponding to a lower ΔE. In this study, the nucleation activity and chain mobility both increased when a small amount of the ICPP was mixed with the HPP, resulting in higher crystallization rates. When 20–40% of the ICPP was added, the n value stated to decrease, which might suggest that the excessive amount of crystal nuclei induced by the higher ICPP content didn't have enough space to grow and the crystal–crystal interactions might increase. But the chain mobility kept improving until 40–60% of the ICPP presented. In combination with the higher nucleation activity, the crystallization rate continued to rise. The maximum crystallization rate was found when the composite contained 60% of the ICPP based on the Avrami-Jeziorny and Mo models. When further increasing the ICPP content, the chain mobility became lower (higher ΔE) and the crystal–crystal interactions increased even more (lower n). Both effects slowed the crystal growth. Although the

Table 5 Correlation analysis results between kinetic parameters and material mechanical and thermal properties

		Tensile MOE	Tensile strength	Flexural MOE	Flexural strength	Notched impact strength	Unnotched impact strength	DSC cooling onset	DSC cooling peak	DSC heating peak	DSC heating enthalpy	Crystallinity
Nucleation activity (Ψ)	Correlation coefficient	0.99	0.99	0.95	0.99	− 0.94	− 0.91	− 0.97	− 0.97	− 0.92	0.99	0.99
	p-value	0.00033	0.00015	0.0033	0.000038	0.0046	0.012	0.00098	0.0016	0.0090	0.000098	0.00025
Avrami exponent n @ 10 °C min^{-1}	Correlation coefficient	0.76	0.79	0.71	0.83	− 0.84	− 0.79	− 0.81	− 0.84	− 0.76	0.79	0.79
	p-value	0.079	0.059	0.11	0.039	0.034	0.059	0.038	0.036	0.079	0.057	0.062

nucleation activity kept increasing, the crystallization rate started to drop. Nevertheless, the quicker nucleation seemed to ease the decrease in the crystallization rate. The neat ICPP had a similar chain mobility to the neat HPP, but it crystallized quicker than the HPP.

Correlations between the crystallization kinetic parameters and the material mechanical and thermal properties

Correlation analysis was carried out with Microsoft Excel to reveal the relationships between the crystallization kinetic parameters determined in this work and the material mechanical and thermal properties we reported previously [8]. The quantities with high correlation coefficients and low *p*-values are listed in Table 5. The nucleation activity showed the strongest correlations to various mechanical and thermal properties, indicating it affected the material properties the most. The Avrami exponent n also exhibited relatively high correlations to the mechanical and thermal properties, suggesting the geometry of the crystallites affected the final products as well. The crystallization rate showed less influence on the mechanical and thermal properties. High correlation was also found between the $F(T)$ in the Mo model and the Z_c in the Avrami–Jeziorny model. It is reasonable because both parameters imply the crystallization rate in the corresponding models. The results also demonstrated that the conclusions from the two models were consistent with each other.

Conclusions

The Avrami–Jeziorny and Mo models successfully described the crystallization processes of the HPP, ICPP, and their composites. The crystallization rate first increased and then decreased with the increase of the ICPP content. The highest crystallization rate was observed when 60 mass% ICPP was mixed with 40 mass% of HPP. The nucleation activity kept increasing when more ICPP presented, demonstrating that the rubber phase in the ICPP acted as a nucleating agent and prompted the crystallization process for the composites. When the ICPP content exceeded 60 mass%, the crystallization rate decreased. It could be caused by the decrease in polymer chain mobility, which was demonstrated by the rising crystallization activation energy, and the increase in crystal–crystal interactions. The nucleation activity was highly correlated with the mechanical and thermal properties of the neat polymers and their composites. The Avrami exponent, *n*, also exhibited relatively high correlations to these properties. The is one mistake. The "Ozawa equation" is a section heading. It should be the same level as the "Jeziorny theory" and "Mo equation".

Acknowledgements This work was performed under the financial assistance award 70NANB20H147 from the National Institute of Standards and Technology, U.S. Department of Commerce. This work is also supported by the Alabama Agricultural Experiment Station and the Hatch program of the National Institute of Food and Agriculture, U.S. Department of Agriculture [ALA031-1-19091]. The authors would also like to thank ExxonMobil Chemical Company for providing the polymer pellets for this research.

Author contributions PW was involved in investigation; data curation; methodology; validation; visualization; writing—original draft; writing—review and editing. YW was involved in conceptualization; methodology; data curation; writing—review and editing. XW contributed to data curation; validation; writing—review and editing. YP contributed to conceptualization; methodology; data curation; resources; supervision; funding acquisition; writing—review and editing. SL was involved in conceptualization; methodology; data curation; resources; supervision; funding acquisition; writing—review and editing. All authors critically reviewed the manuscript and approved the final version.

Declarations

Conflict of interest The authors declare that they have no conflict of interest.

References

1. Maddah HA. Polypropylene as a promising plastic: a review. Am J Polym Sci. 2016;6:1–11. https://doi.org/10.5923/j.ajps.20160601.01.
2. Mileva D, Tranchida D, Gahleitner M. Designing polymer crystallinity: an industrial perspective. Polym Cryst. 2018;1:e10009. https://doi.org/10.1002/pcr2.10009.
3. Karian H. Handbook of polypropylene and polypropylene composites, revised and expanded. Boca Raton: CRC press; 2003.
4. Liang J, Li R. Rubber toughening in polypropylene: a review. J Appl Polym Sci. 2000;77:409–17. https://doi.org/10.1002/(SICI)1097-4628(20000711)77:2%3c409::AID-APP18%3e3.0.CO;2-N.
5. Mirabella FM Jr. Impact polypropylene copolymers: fractionation and structural characterization. Polym. 1993;34:1729–35. https://doi.org/10.1016/0032-3861(93)90333-6.
6. Magagula SI, Ndiripo A, JohannesvanReenen A. Heterophasic ethylene-propylene copolymers: New insights on complex microstructure by combined molar mass fractionation and high temperature liquid chromatography. Polym Degrad Stab. 2020;171:109022. https://doi.org/10.1016/j.polymdegradstab.2019.109022.
7. Hodgkinson J, Savadori A, Williams J. A fracture mechanics analysis of polypropylene/rubber blends. J Mater Sci. 1983;18:2319–36. https://doi.org/10.1007/BF00541836.
8. Peng Y, Liu S, Wang P, Wang Y, Wang X. Formulating polypropylene with desired mechanical properties through melt compounding of homopolymer and impact copolymer. Polym Cryst. 2022;2022:3084446. https://doi.org/10.1155/2022/3084446.
9. Dal Castel C, Pelegrini T Jr, Barbosa R, Liberman S, Mauler R. Properties of silane grafted polypropylene/montmorillonite nanocomposites. Compos Part A Appl Sci. 2010;41:185–91. https://doi.org/10.1016/j.compositesa.2009.09.017.
10. Causin V, Marega C, Marigo A, Ferrara G, Ferraro A. Morphological and structural characterization of polypropylene/conductive graphite nanocomposites. Eur Polym J. 2006;42:3153–61. https://doi.org/10.1016/j.eurpolymj.2006.08.017.

11. Tjong SC, Xu SA. Non-isothermal crystallization kinetics of calcium carbonate-filled β-crystalline phase polypropylene composites. Polym Int. 1997;44:95–103. https://doi.org/10.1002/(SICI)1097-0126(199709)44:1%3c95::AID-PI821%3e3.0.CO;2-L.
12. Ferreira C, Dal Castel C, Oviedo M, Mauler R. Isothermal and non-isothermal crystallization kinetics of polypropylene/exfoliated graphite nanocomposites. Thermochim Acta. 2013;553:40–8. https://doi.org/10.1016/j.tca.2012.11.025.
13. Blázquez J, Conde C, Conde A. Non-isothermal approach to isokinetic crystallization processes: application to the nanocrystallization of HITPERM alloys. Acta Mater. 2005;53:2305–11. https://doi.org/10.1016/j.actamat.2005.01.037.
14. Liu T, Mo Z, Wang S, Zhang H. Isothermal melt and cold crystallization kinetics of poly (aryl ether ether ketone ketone)(PEEKK). Eur Polym J. 1997;33:1405–14. https://doi.org/10.1063/1.4949642.
15. Jeziorny A. Parameters characterizing the kinetics of the non-isothermal crystallization of poly (ethylene terephthalate) determined by DSC. Polym. 1978;19:1142–4. https://doi.org/10.1016/0032-3861(78)90060-5.
16. Ozawa T. Kinetic analysis of derivative curves in thermal analysis. J Therm Anal. 1970;2:301–24. https://doi.org/10.1007/BF01911411.
17. Ozawa T. Kinetics of non-isothermal crystallization. Polym. 1971;12:150–8. https://doi.org/10.1016/0032-3861(71)90041-3.
18. Jayasree T, Predeep P. Non-isothermal crystallization behavior of Styrene butadiene rubber/high density polyethylene binary blends. J Therm Anal Calorim. 2012;108:1151–60. https://doi.org/10.1007/s10973-012-2257-y.
19. Alvarez VA, Pérez CJ. Effect of different inorganic filler over isothermal and non-isothermal crystallization of polypropylene homopolymer. J Therm Anal Calorim. 2012;107:633–43. https://doi.org/10.1007/s10973-011-1705-4.
20. Alghyamah AA, Elnour AY, Shaikh H, Haider S, Poulose AM, Al-Zahrani S, et al. Biochar/polypropylene composites: a study on the effect of pyrolysis temperature on crystallization kinetics, crystalline structure, and thermal stability. J King Saud Univ Sci. 2021;33:101409. https://doi.org/10.1016/j.jksus.2021.101409.
21. Qiao Y, Jalali A, Yang J, Chen Y, Wang S, Jiang Y, et al. Non-isothermal crystallization kinetics of polypropylene/polytetrafluoroethylene fibrillated composites. J Mater Sci. 2021;56:3562–75. https://doi.org/10.1007/s10853-020-05328-5.
22. Wang S, Zhang J. Non-isothermal crystallization kinetics of high density polyethylene/titanium dioxide composites via melt blending. J Therm Anal Calorim. 2014;115:63–71. https://doi.org/10.1007/s10973-013-3241-x.
23. Menezes BRCd, Campos TMB, Montanheiro TLdA, Ribas RG, Cividanes LdS, Thim GP. Non-isothermal crystallization kinetic of polyethylene/carbon nanotubes nanocomposites using an isoconversional method. J Compos Sci. 2019;3:21. https://doi.org/10.3390/jcs3010021.
24. Kourtidou D, Tarani E, Chrysafi I, Menyhard A, Bikiaris DN, Chrissafis K. Non-isothermal crystallization kinetics of graphite-reinforced crosslinked high-density polyethylene composites. J Therm Anal Calorim. 2020;142:1849–61. https://doi.org/10.1007/s10973-020-10085-3.
25. Blaine RL. Determination of polymer crystallinity by DSC. TA123. 2010.
26. Blaine RL. Thermal applications note. Polymer Heats of Fusion. 2002.
27. Yuan Q, Awate S, Misra R. Nonisothermal crystallization behavior of polypropylene–clay nanocomposites. Eur Polym J. 2006;42:1994–2003. https://doi.org/10.1016/j.eurpolymj.2006.03.012.
28. Huang Y, Chen G, Yao Z, Li H, Wu Y. Non-isothermal crystallization behavior of polypropylene with nucleating agents and nano-calcium carbonate. Eur Polym J. 2005;41:2753–60. https://doi.org/10.1016/j.eurpolymj.2005.02.034.
29. Nofar M, Guo Y, Park CB. Double crystal melting peak generation for expanded polypropylene bead foam manufacturing. Ind Eng Chem Res. 2013;52:2297–303. https://doi.org/10.1021/ie302625e.
30. Nofar M, Zhu W, Park C. Effect of dissolved CO2 on the crystallization behavior of linear and branched PLA. Polym. 2012;53:3341–53. https://doi.org/10.1016/j.polymer.2012.04.054.
31. Chen S, Jin J, Zhang J. Non-isothermal crystallization behaviors of poly (4-methyl-pentene-1). J Therm Anal Calorim. 2011;103:229–36. https://doi.org/10.1007/s10973-010-0957-8.
32. Wang J, Dou Q. Non-isothermal crystallization kinetics and morphology of isotactic polypropylene (iPP) nucleated with rosin-based nucleating agents. J Macromol Sci Phys. 2007;46:987–1001. https://doi.org/10.1080/00222340701457311.
33. Buzarovska A. Crystallization of polymers (2nd edition) Volume 2: Kinetics and mechanisms. Edited by Leo Mandelkern. Cambridge University Press, Cambridge, 2004. ISBN 0 521 81682 3. pp 478. Polym Int. 2005;54:1466–7. https://doi.org/10.1002/pi.1883
34. Zhang J, Chen S, Jin J, Shi X, Wang X, Xu Z. Non-isothermal melt crystallization kinetics for ethylene–acrylic acid copolymer in diluents via thermally induced phase separation. J Therm Anal Calorim. 2010;101:243–54. https://doi.org/10.1007/s10973-009-0619-x.
35. Kissinger HE. Variation of peak temperature with heating rate in differential thermal analysis. J Res Natl Bur Stand. 1956;57:217–21. https://doi.org/10.6028/jres.057.026.
36. Dobreva A, Gutzow I. Activity of substrates in the catalyzed nucleation of glass-forming melts. II. Experimental evidence. J Non-Cryst Solids. 1993;162:13–25. https://doi.org/10.1016/0022-3093(93)90737-I.